Microwave measurements, calculations, and analysis for the gas phase ammonia-formic acid dimer

Kristen K. Roehling, Jack L. Nichols, Adam M. Daly, Stephen G. Kukolich[a]

Department of Chemistry and Biochemistry, University of Arizona

1306 E. University Avenue, Tucson AZ 85721

Abstract

The gas-phase doubly hydrogen-bonded formic acid-ammonia complex was obtained by heating a sample of ammonium formate in neon. High-level DFT and MP2 calculations with various basis sets were performed and barriers for proton tunneling and internal rotation were determined. The microwave spectrum was measured in the 7-16 GHz frequency range using a Flygare-Balle type pulsed beam Fourier transform microwave (FTMW) spectrometer. Double resonance transitions were observed near 20 GHz. Rotational transitions were measured and fitted for two vibrational states to obtain the rotational constants and quadrupole coupling constants. The rotational constants were (JN) determined to have the following values: A = 12017.0(2), B = 4337.331(2), and C = 3227.279(2) for the 0^+ state and A = 12017.0, B = 4302.02(1), and C = 3238.161(1) for the 0^- state and have been fit to 16 transitions and 9 transitions

[a] kukolich@arizona.edu

respectively. Each state was fit to a rigid model showing quadrupole splitting and compared with computations.

1. Introduction

We report the first measurements of the gas phase dimer consisting of formic acid and ammonia. The structure is most consistent with the microwave absorptions made from 7.5 GHz to 22 GHz. This complex is a doubly hydrogen-bonded dimer that exhibits evidence of a large amplitude motion through double proton tunneling. To our knowledge, this is the first evidence of a complex with hydrogen bond donation by a N-H group showing proton exchange studied by microwave spectroscopy.

Doubly hydrogen-bonded complexes can provide simple models for hydrogen bonding present in DNA base pairs. The DNA base pair A-T, with two hydrogen bonds, and G-C, with three hydrogen bonds, both have N-H hydrogen bonds. Microwave measurements on the formic acid-ammonia complex provide another opportunity to study the structure and dynamics of a doubly H-bonded complex with N-H bonds and C_{2v}(m) symmetry. Doubly hydrogen-bonded carboxylic acids with C_{2v}(m) symmetry[1] can exhibit interesting tunneling dynamics. The C_{2v}(m) symmetry for the complex makes the two O atoms in the complex equivalent. The simplest carboxylic acid system observed using microwave spectroscopy, the HCOOH—DCOOH[2] (AD) dimer and other carboxylic acid complexes, propiolic acid – formic acid,[3,4,5] nitric acid – formic acid[6], benzoic acid – acetic acid[7] and acetic acid – formic acid[8] have the C_{2v}(m) symmetry and have been shown to exhibit resolvable concerted proton tunneling splittings in microwave spectra. Without the

C_{2v}(m) symmetry, tunneling splittings have not been observed. No tunneling splittings were reported for formic acid-formamide,[9] 1,2-cyclohexanedione-formic acid[10], cyclopropanecarboxylic acid-formic acid,[11] or the maleimide – formic acid complex.[12]

Since the publication of the (JN) formic acid—argon dimer,[13] many gas phase dimers of formic acid have been used to study strongly bound complexes that exhibit interactions with biological relevance. The structure of the formamide—formic acid complex[9] was consistent with a N-H --- O bond, but no evidence of tunneling was observed. The only amine published with formic acid, the (JN) trimethylamine—formic acid dimer, (JN) consists of only one hydrogen bond along the C-O-H --- N, and the authors did not report any evidence of tunneling.[14]

Ammonia is considered to be the only base in the atmosphere and several studies have been published to analyze the structure and reactive pathways with carboxylic acids.[15,16] To date, only infrared spectroscopy has been used to study the complex of the ammonia—formic acid dimer[17]. In that study, the complex is modeled as a singly hydrogen-bonded complex leading to proton transfer to produce ammonium formate. Proton tunneling dynamics has been proposed to be an important aspect of mutation in DNA base pairs[18,19] and continues to drive studies since the observation of double hydrogen exchange in the formic acid dimer using infrared spectroscopy[20] and the first observation in propiolic acid – formic acid dimer using microwave spectroscopy.[3]

The microwave spectrum of ammonia has a special place in spectroscopy and the ammonia dimer has been the focus of many studies due to the ambiguity of the gas phase structure.[21,22,23,24] The result of our work indicates that ammonia is not only capable of hydrogen bonding but will undergo double proton exchange in symmetric environments.

The classic double-well and the structures of the equilibrium and transition states are shown in Figure 1.

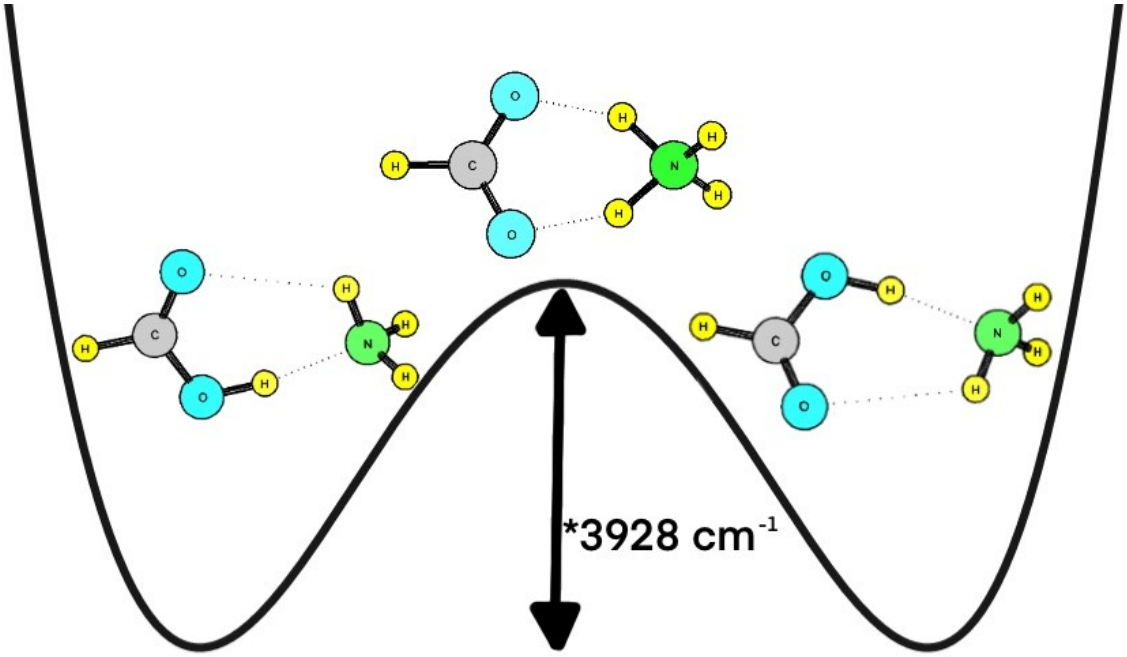

Figure 1. (KR) Double-well potential showing the stable asymmetric state and the transient, higher energy symmetric state. The potential energy difference between the structures is the barrier to double proton tunneling. * value obtained from B3LYP/6-311++G** calculations

2. Experimental

Initial measurements of rotational transitions were obtained for the formic acid-ammonia dimer system in the 7.5-16.2 GHz range using the Flygare-Balle type pulsed-beam Fourier transform microwave spectrometer that was previously described at the University of Arizona.[25] Final measurements were made using a recently constructed

Flygare-Balle type pulsed beam Fourier transform microwave spectrometer fitted with a coaxial valve in a fixed mirror. The control program was written in LabView to manage the precise timing of multiple free induction decay (multi-FID) acquisitions with a Picoscope 2204A. A National Instrument 6602 timing pulse board was used to produce the four 1-microsecond pulses spaced by 100 microseconds that were sent to the microwave switch (Herley-MDI MD-012C044) and then traveled via coaxial cable into the cavity resonator. The entire 400-microsecond window is digitized at 6.125 MHz. One acquisition is composed of two microwave pulses: one with and one without a valve pulse. (JN) The difference between these pulses is sliced into 4 sections and added together in software. The mode is tracked using a National Instrument 6024 card digitizer that records the response of the reflected microwave signal using a homodyne mixing circuit described earlier.[25] Results from the scans were analyzed using a signal processing program written in MATLAB to visualize the results from scans that include several hundred files. Measurements reported in this paper were saved at multiple frequencies and the doppler doubled signals were measured in an analysis program using the results of a fast Fourier transform and reported as the average of the doppler components. An example of the recorded spectrum with a microwave frequency of 15017.2 GHz is given in Figure 2.

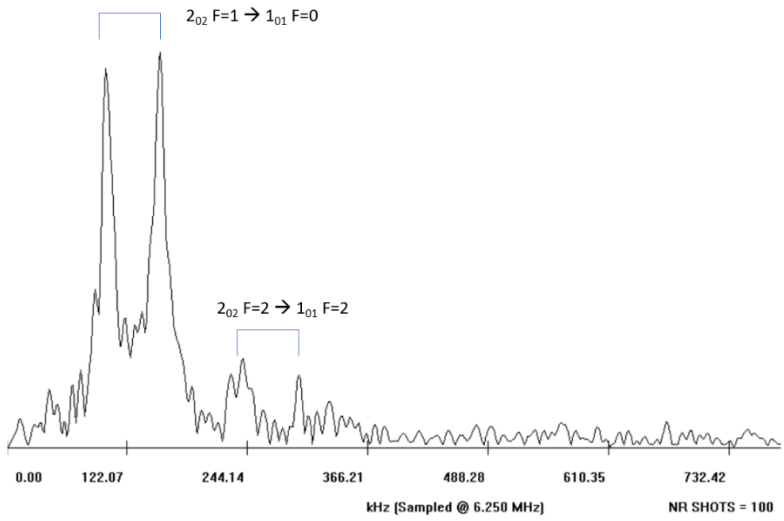

Figure 2. Direct Measurement of two components of the $2_{02} \rightarrow 1_{01}$ transition with doppler doubling present taken using a microwave stimulation frequency of 15017.2 MHz.

Formic acid-ammonium salt (Ammonium formate) (97%) was purchased from Sigma-Aldrich and used without any further purification. To produce the vapor pressure required for sufficient signal strength, the formic acid-ammonium salt was loaded into a glass sample cell that was heated to about 35 ˚C. One end of the sample cell was connected to the pulsed valve of the microwave spectrometer, and the other end was connected to a gas-handling system that used argon as the carrier gas. The system was maintained at a backing pressure of 1 atm. The pressure inside the cavity of the spectrometer was maintained in the range of 10^{-6} torr to 10^{-7} torr using a diffusion pump. Using a General Valve pulsed valve mounted to the fixed mirror, the molecules were pulsed into the chamber at a frequency of 2 Hz.

To measure rotational transitions in the range of 20.9-22.2 GHz, the method of microwave-microwave double resonance was used[26]. For this method, a secondary system is required which consists of an HP8673 synthesizer controlled by a new National Instruments' LabVIEW program. This program controls the synthesizer to

introduce the probe signal through microwave cabling and is connected to a microwave horn position above the diffusion pump pointed at a 90-degree orientation to the coaxial molecular beam. The result from the original multi-FID signal is split and passed to a Picoscope 5302 digitizer. The same signal processing mentioned previously is performed to extract the molecular signal from the background. The fast Fourier transform is analyzed with and without the secondary microwave signal present (two channels), and the result of each is analyzed in three different ways by plotting the following: ratio of maximum values, ratio of integrated values (signal strength vs frequency in the range covering the doppler doublet) and ratio of sums (signal strength summed across the range covering the doppler doublet) vs frequency. All three are plotted as the ratio of the secondary microwave source OFF to the secondary microwave ON vs frequency and used to assign the resonant frequency. An example highlighting the efficacy of the double resonance instrument in connecting rotational transitions is shown in Figure 3, which depicts a double resonance experiment connecting the signals of 15017 MHz and 7564.6 MHz that share the common energy level, 1_{01} F=1. Both synthesizers used in double resonance were referenced to a quartz oscillator tuned to a standard Rubidium 10 MHz source.

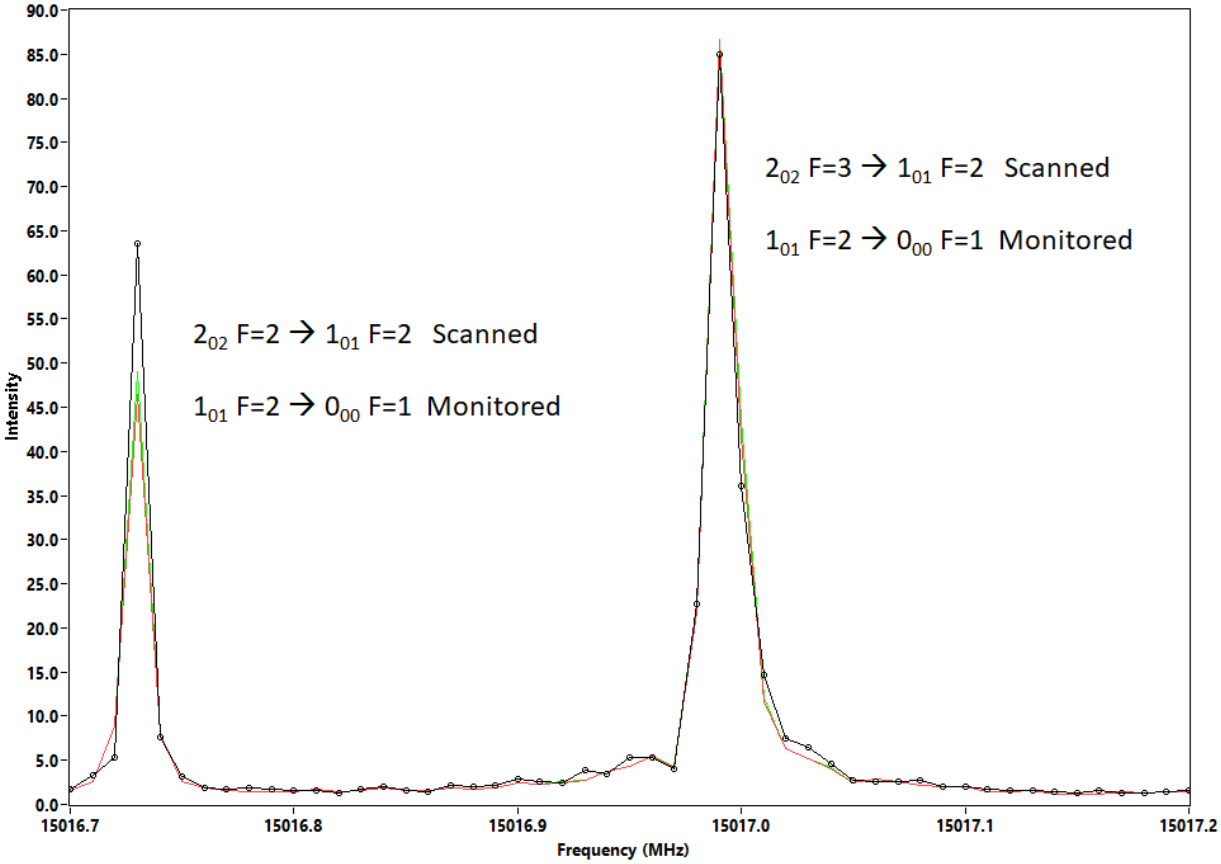

Figure 3. (JN) Spectrum showing the result of microwave-microwave double resonance confirmation that the signals of 7564.6 and 15017 share a common energy level, 1_{01} F= 1. Power used in the probe (scanned) (15.017 GHz) was 13 dBm.

3. Computational

Structural parameters, rotational constants, the barrier to tunneling, and binding energy were calculated using Gaussian G-16[27] on the University of Arizona HPC system. The calculations were done on the Ocelote HPC, 28 processor system using 268 Gb of memory. For the Gaussian-16 suites (G-16), the keyword “output=picket” provides microwave parameters. These parameters include A, B, C, and quadrupole

coupling constants for N-14. Methods used for the calculations below are B3LYP[28], B97D[29], M11[30], wB97XD[31], MP2[32], and M06[33]. The basis sets utilized below are 6-31G*[34], 6-31++G**[35], 6-311++G**[36], def2-QZVPP[37], aug-cc-pVDZ[38], aug-cc-pVTZ[39], aug-cc-pVQZ[40], cc-pVDZ[41], and cc-pVTZ[42]. The calculated rotational constants and various parameters of interest are provided in Table 1. Notably, the method B3LYP with the 6-311++G** basis set yielded estimates of ammonium formate rotational constants closest to the experimental values.

Results of the calculations are shown in Tables 1 And 2. (below):

Table 1. (KR) The experimental and calculated parameters of ammonium formate. Frequencies are in MHz.

Parameter	1. Experimental (lower state, 0^+)	2. Experimental (upper state, 0^-)	3. B3LYP	4. B97D	5. M11	6. B97D	7. wB97XD	8. MP2	9. MP2
Basis set	-	-	a	b	c	d	e	f	d
Number of fit transitions	16	9	-	-	-	-	-	-	-
A	12017.0(3)	12017.0(2)*	12003.9	11723.2	11963.2	11852.3	11781.8	11801.8	11882.9
B	4337.331(3)	4302.02(8)	4289.9	4422.8	4511.9	4384.4	4617.4	4517.0	4492.4
C	3227.279(3)	3238.16(7)	3214.9	3268.0	3335.0	3256.5	3377.5	3324.1	3317.2
1.5 χ_{aa} (N1)	-0.9608(102)	-0.8896(610)	-1.22	-0.76	-0.64	-0.87	-0.45	-0.55	-0.67

0.25(χ_{bb}-χ_{cc})(N1)	-0.72490(538)	-0.830(249)	-0.85	-0.82	-1.04	-0.87	-0.95	-0.88	-0.84
μ_a(Debye)	-	-	-2.82	-2.85	-2.32	-2.84	-2.77	-2.53	-2.49
μ_b(Debye)	-	-	-0.24	-0.23	-0.36	-0.27	-0.07	-0.13	-0.22
X_{aa}(N1)	-.64(1)	-0.56(4)	-0.81	-0.50	-0.43	-0.62	-0.30	-0.37	-0.45
χ_{bb}(N1)	-1.1(1)	-1.4(4)	-1.29	-1.38	-1.86	-1.43	-1.74	-1.57	-1.46
χ_{cc}(N1)	1.8(1)	1.9(4)	2.10	1.89	2.29	2.05	2.04	1.94	1.90
σ(kHz)	61	333	-	-	-	-	-	-	-

a. 6-311++G** b. aug-cc-pVDZ c. def2-QZVPP d. aug-cc-pVQZ e. 6-31G* f. cc-pVTZ

* fixed to lower, 0^+ state

All errors reported were obtained using PIFORM avaliable at http://www.ifpan.edu.pl/~kisiel/asym/asym.htm#piform(AD)

Table 2. Energy comparison between optimized symmetric and asymmetric structures to calculate the barrier to proton tunneling.

Method/basis set	Symmetric energy (hartrees)	Asymmetric energy (hartrees)	Barrier (symmetric energy - asymmetric energy) (cm^{-1})
B3LYP/6-311++G**	-246.4115	-246.4294	3928.113
M11/cc-pVDZ	-246.2295	-246.2445	3274.561

M06/6-31++G**	-246.2106	-246.2293	4110.738
B97D/aug-cc-pVTZ	-246.2873	-246.3045	3777.378
MP2/aug-cc-pVDZ	-245.7343	-245.7510	3660.420
MP2/cc-pVTZ	-245.9266	-245.9450	4036.555

Calculations with two different starting geometries were performed to estimate the barrier to double proton tunneling in Table 2. For reference with the simplest carboxylic acid system studied, DCOOH—HCOOH, the barrier to proton tunneling was calculated to be 2500 cm^{-1} [43].(AD) The asymmetric structure reflects the lowest energy configuration (or isomer) where one proton is closer to ammonia and the other is closer to formic acid. The symmetric, transition state structure represents the complex mid-tunneling where both protons are between ammonia and formic acid. These structures are shown in Figure 4.

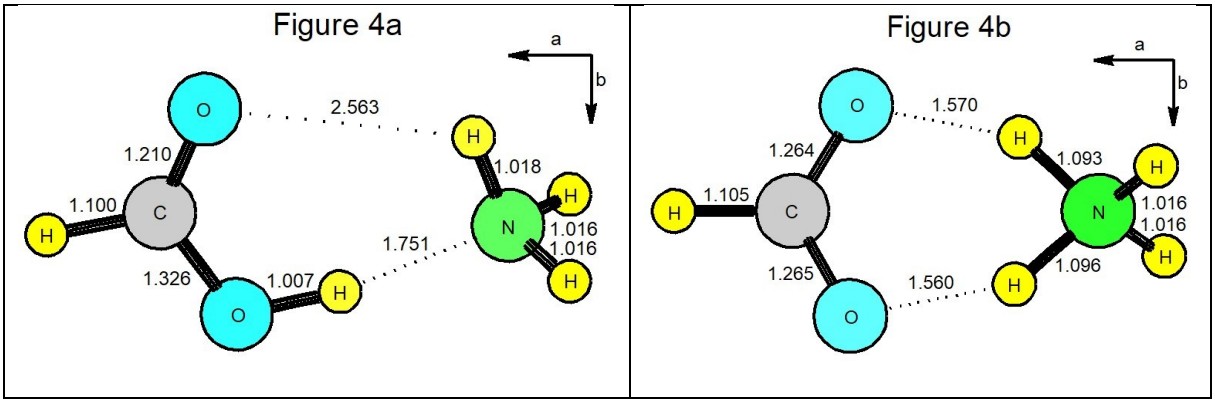

Figure 4 a and b. The structure of the lowest energy (left) and the symmetric transient (right) forms of ammonium formate. The structures were obtained from the optimized geometries using B3LYP/6-311++G**.

Two starting geometries were used in the calculations reported in this paper. When starting with an initial asymmetric structure, an optimized asymmetric structure was obtained, and beginning with an initial symmetric structure yielded an optimized symmetric structure. The two structures are shown in Figures 4a and 4b. No additional parameters were used in Gaussian to obtain the symmetric state due to the convergence to the symmetric geometry. An imaginary frequency was obtained at the symmetric geometry confirming its identity as a transition state. (KR\AD)

Several DFT methods were used to explore the range of energy barrier values: M11, B3LYP, wB97XD, and M06. Two basis sets were used: 6-311++G**, the triple zeta set of Pople with polarized and diffuse functions on each atom, and cc-pVDZ, the correlation consistent double zeta function with polarization. MP2 calculations were also done as shown in Tables 1. and 2. The calculated asymmetric structure energies

are smaller than the symmetric structure energies. These energies can be used to estimate the barrier to tunneling to be between 3274 cm^{-1} and 4110 cm^{-1} as described in Table 2 (KR).

The binding energy of the dimer was estimated using the method and basis set that most accurately estimated the experimental rotational constants. Using the density-functional theory method B3LYP and the 6-311++G** basis set, the calculated binding energy is 4197 cm^{-1}. Estimations of binding energies were calculated using a variety of methods and basis sets. All binding energy calculations were performed using the Gaussian Counterpoise keyword. (KR) The calculated binding energies range from 3973 cm^{-1} to 4683 cm^{-1}, as shown in Table 3 below.

Table 3. (KR) Calculated binding energies for two possible isomers of the ammonium formate dimer.

Method/basis set	Corrected binding energy (cm^{-1})
B3LYP/6-311++G**	4197
M06/6-31++G**	4683
MP2/aug-cc-pVDZ	3973
MP2/cc-pVTZ	4092

The energies of the structure in Figure 4a and an alternative isomer are shown in Table 4. The trans formic acid dimer with ammonia would exhibit a single hydrogen bond. However, the energy of the cis formic structure is calculated to be about 1650-1884 (cm^{-1}) lower than the trans structure. The calculated rotational constants for

the trans isomer are very different than the experimental rotational constants shown in Table 1. The calculated trans structure's rotational constants using B3LYP with 6-311++G** are A = 35836 MHz, B = 2426 MHz, and C = 2300 MHz. Both the lower energy of the cis isomer and different rotational constants indicate that the trans isomer is not a likely structure for ammonium formate. (KR)

Table 4. Calculated isomer energy difference between the cis and trans isomers of the ammonium formate dimer. (KR)

Method/basis set	(Trans-cis) isomer energies (cm^-1)
B3LYP/6-311++G**	1651
M06/6-31++G**	1884
MP2/aug-cc-pVDZ	1672

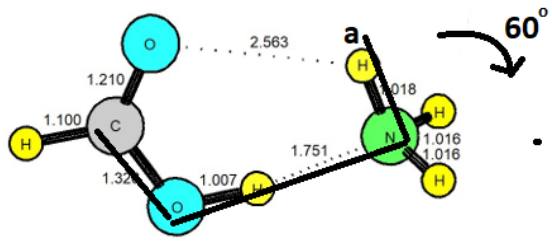

In an effort to provide information regarding an alternative explanation for the internal motion in the formic acid – ammonia dimer, the internal rotation of ammonia has been calculated using two different methods. M06/6-31++G** and MP2/cc-pVTZ methods were used to estimate the barrier to internal rotation by performing a single point calculation of the structure resulting from rotation of the dihedral (C-O-N-H(in a-b plane)) angle as shown in the figure XX. The dihedral (C-O-N-H(in a-b plane)) angle for the optimized structure is zero. The angle was rotated (all H-atoms move, nitrogen is fixed) and a single point energy calculation with the angle set to 60 degrees. The energy increase was calculated to be 1942 cm^{-1} and 2040 cm^{-1} for the M06/6-31++G** and MP2/cc-pVTZ methods respectively. Although this motion has not been observed in other double hydrogen bonded carboxylic acid dimers, the high mass atoms most likely prevent this type of interal motion. Interal rotation motion can not be excluded from possibly occurring in this complex and adds an additional complexity in the analysis of the spectrum.(AD)

Analysis

Using the predictions in Table 1, The initial A, B, and C rotational constants from the predictions in Table 1 were used in Pickett's SPCAT[44] program to predict the a-dipole pure rotational spectrum. Large scans were conducted in the region of 7400 – 7700 MHz where a doublet showing quadrupole splitting from the nitrogen atom (I =1) and was observed centered at 7540 and 7564 MHz. These transitions were assigned to the $1_{01} \rightarrow 0_{00}$ to the two states 0^+ and 0^-. A scaling factor was calculated and a scan at 15 GHz was performed to find the $2_{02} \rightarrow 1_{01}$ and a second set of doublets with characteristic quadrupole splitting was observed, see Figure 2. Several attempts were made to measure the $2_{12} \rightarrow 1_{11}$, predicted near 14000 MHz (JN). A single set of signals indicative of nuclear quadrupole was observed. This procedure was repeated for the transition at $2_{11} \rightarrow 1_{10}$ and a single set of signals was observed, similar to the $2_{12} \rightarrow 1_{11}$ transition. Based on the measurements within the Ka = 0 ladder, a doublet separated by ~25 MHz was expected but only one transition was observed. Each region was rescanned to observe the missing transition, but the nearest signals detected were several hundred MHz away from the transition measured for both $2_{12} \rightarrow 1_{11}$ and $2_{11} \rightarrow 1_{10}$. Both sets of signals, 14019 and 16239, were assigned to transitions to the 0^+ state with the signals from the 7564 MHz transition assigned to $1_{01} \rightarrow 0_{00}$ and 15017 assigned to $2_{02} \rightarrow 1_{01}$. The recorded frequencies are given in Table 5 (KR).

The transitions measured at 7540 and 14977 showing characteristic quadrupole coupling patterns were assigned to another state, 0^- for the $1_{01} \rightarrow 0_{00}$ and $2_{02} \rightarrow 1_{01}$ transitions, respectively. No other direct transitions to this state were assigned to this state. The assigned transitions were used in the SPFIT program contained in Pickett's program suite[44] to obtain experimental rotational constants as well as quadrupole coupling constants. The fit results are listed in Tables 4 and 5.

The recorded frequencies for the lower state are given in Table 5 (JN)(KR).

Table 5. (KR, sig figs) Fit of lower state using direct and double resonance measurements. J 0→1 and 1→2 (FTMW, uncertainty 10 kHz) and J 2→3 (Double resonance, uncertainty 100 kHz) using SPFIT to the constants in Table 1.

J_{KaKc}'	F'	J_{KaKc}"	F"	Measured (MHz)	Model (MHz)	Obs-calc (kHz)
1_{01}	1	0_{00}	1	7564.3975	7564.3994	-1.9
1_{01}	2	0_{00}	1	7564.5911	7564.5915	-0.4
1_{01}	0	0_{00}	1	7564.8857	7564.8795	6.2
2_{02}	2	1_{01}	2	15016.7239	15016.7266	-2.7
2_{02}	1	1_{01}	0	15016.8560	15016.8535	2.5
2_{02}	3	1_{01}	2	15016.9908	15016.9934	-2.6

2_{02}	1	1_{01}	1	15017.3354	15017.3337	1.7
2_{12}	2	1_{11}	2	14018.2634	14018.2638	-0.4
2_{12}	2	1_{11}	1	14018.6037	14018.6027	1.0
2_{12}	3	1_{11}	2	14018.8262	14018.8327	-6.5
2_{12}	1	1_{11}	1	14019.4922	14019.4877	4.5
2_{11}	1	1_{10}	0	16239.4600	16239.4694	-9.4
2_{11}	3	1_{10}	2	16238.8800*	16238.8746	5.5
2_{11}	2	1_{10}	1	16238.7100*	16238.7066	3.4
3_{13}	4	2_{12}	3	20960.95	20960.72	230
3_{03}	4	2_{02}	3	22252.53	22252.45	80

*These transitions frequencies were obtained from direct measurement and are reported to 10 kHz uncertainty. (AD)

Table 6. (KR, sig figs) Fit of upper state using direct and double resonance measurements. J 0→1 and 1→2 (FTMW, uncertainty 10 kHz) and J 2→3 (Double resonance, uncertainty 100 kHz) using SPFIT to the constants in Table 1.

J_{KaKc}'	F'	J_{KaKc}"	F"	Measured (MHz)	Model (MHz)	Obs-calc (kHz)
1_{01}	1	0_{00}	1	7539.9712	7539.9822	-11.0
1_{01}	2	0_{00}	1	7540.1563	7540.1601	-3.8
1_{01}	0	0_{00}	1	7540.4302	7540.4270	3.2
2_{02}	2	1_{01}	2	14977.1289	14977.1169	12.0
2_{02}	2	1_{01}	1	14977.2832	14977.2948	-11.6
2_{02}	3	1_{01}	2	14977.3916	14977.3747	16.9

2_{02}	1	1_{01}	2	14977.5078	14977.5180	-10.2
2_{02}	1	1_{01}	1	14977.6982	14977.6959	2.3
3_{03}	3	2_{02}	2	22213.87	22214.85	-980

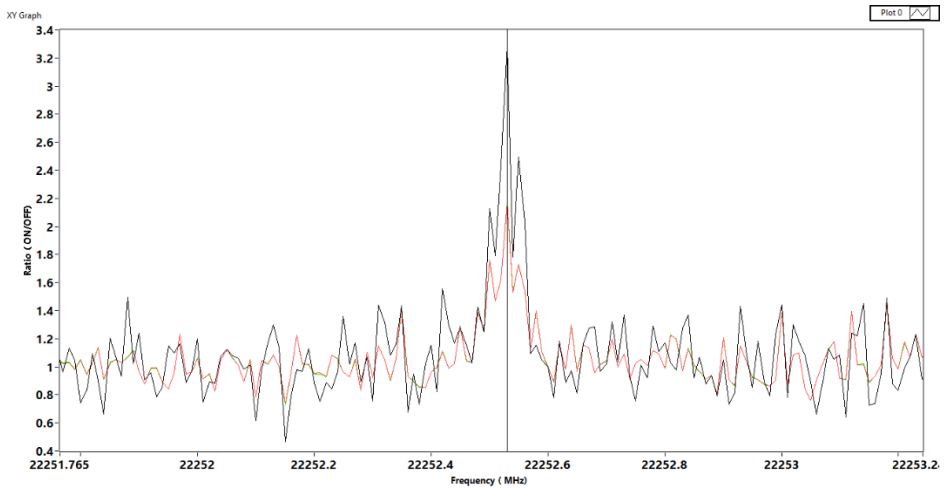

Figure 5. Ratio of OFF to ON microwave – microwave resonance signal at 22252.53 MHz while monitoring 15017.95 MHz.

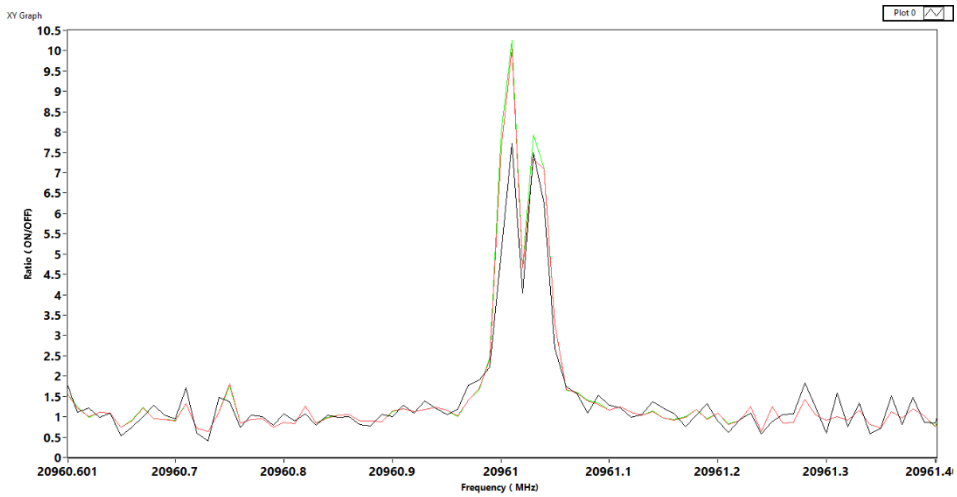

Figure 6. Ratio of OFF to ON microwave – microwave resonance signal at 20961.02 MHz while monitoring 14018.95 MHz.

4. Discussion

a-dipole spectrum

Using the results of the fit to 5 constants, including the three rotational constants (A, B, and C) and two quadrupole coupling constants terms, $1.5\chi_{aa}$ and $0.25(\chi_{bb} - \chi_{cc})$ in SPFIT[44], predictions for the $3_{03} \rightarrow 2_{02}$ and $3_{13} \rightarrow 2_{12}$ were made and found to be at 22.2 and 20.9 GHz using microwave-microwave double resonance. This technique was especially useful in the confirmation that there were two states, 0^+ and 0^-. While monitoring the 1_{01} (F=2) $\leftarrow$ 0_{00} (F=1) transition at 7564.591 MHz, scans of 15017 GHz were shown to interfere with the signal. Not only were we able to confirm the level

connection, but we were also able to extend the range of our spectrometer to 22 GHz by monitoring the 2_{02} (F=2) → 1_{01} (F=1) at 15017 MHz. A summary of the transitions observed (or confirmed) using double resonance is given in Figure 7. A sixth constant, D_J, was found to be necessary to fit the lower state data to measurement uncertainties.

The root mean square of (observed – calculated) is given to be 60 kHz for the 0+ state. The largest contribution to this error come from the double resonance measurements which are estimated to have an uncertainty in determination of the frequency to be 100 kHz. Direct measurements are much better fit where the maximum deviation from the predicted frequency is observed at 9.4 kHz. (AD)

The 0^- state remains an open investigation since we are unable to fit or find the 2_{12}→1_{11} and 2_{11} → 1_{10} transitions. Initially, we tried both of the detected transitions with the signals at 7540 MHz assigned to 1_{01}→ 0_{00} and 14977 assigned to 2_{02} → 1_{01} but were unable to obtain a reasonable fit. The standard deviation of 333 kHz is high but most of the variation comes from the measurement of the 3_{03} → 2_{02} transition using double resonance and using the A rotational constant of the lower state. Additional transitions at higher J would greatly improve the fit but are out of our frequency range.

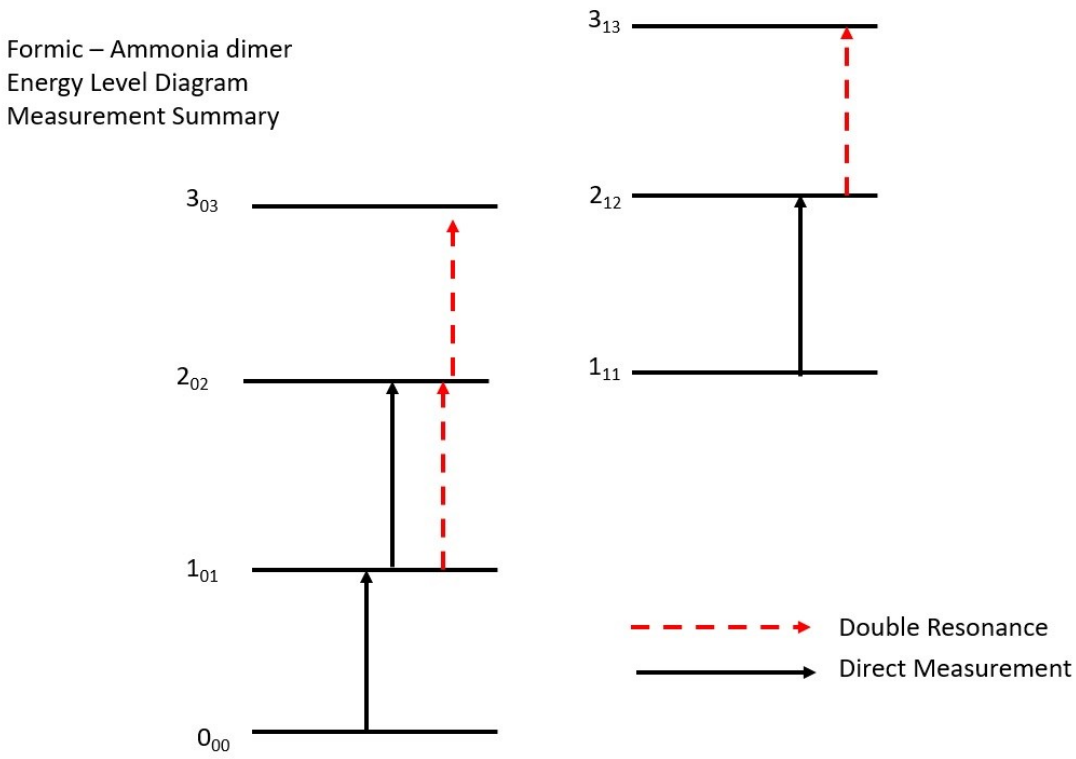

Figure 7. Energy level diagram indicating transitions measured by direct measurement and microwave-microwave double resonance. $2_{02} \rightarrow 1_{01}$ was measured using both methods to verify connectivity but direct measurements were used in the fit.

Microwave – Microwave double resonance experiments

We utilized microwave–microwave double resonance to detect transitions J=3 → J=2. A total of three transitions were included in the two fits that greatly improved our confidence in our assignments, see Figure 7. Using the system described in the experimental section, initial tests were performed using the monitor signal at 7564.591 MHz and the region of 15017 MHz was scanned. Very strong signal depletions were obtained by taking the ratio of the integrated signals of the microwave probe power OFF to microwave probe power ON, see Figure 3. Next, scans were made at 22200 MHz

while monitoring the 15017.017 MHz signal, and a positive detection was obtained and included in the fit as the $3_{03} \rightarrow 2_{02}$ transition frequency. The characteristic signal is shown in Figure 5 with off-resonance oscillating about 1.0 and on-resonance increasing to 3.3. The same procedure was performed at 20.9 GHz while monitoring 14018.95 MHz and the on-resonance signal was 10.5, see Figure 6. The increased signal for the $3_{13} \rightarrow 2_{12}$ detection relative to $3_{03} \rightarrow 2_{02}$ is thought to be due to the higher power levels in our system at 20960 MHz vs 22200 MHz.

Measurements were made with the 0^- state to verify that the signals at 7540 MHz and 14977 are connected through a shared energy level, 1_{11}. Unfortunately, neither transition shares a common energy level with the missing $2_{12} \rightarrow 1_{11}$ or $2_{11} \rightarrow 1_{10}$ transitions. We are able to obtain fits to χ_{aa}, χ_{bb}, and χ_{cc} for the 0^- state. Interestingly, we observe that there is an increase in χ_{bb} with respect to the nitrogen quadrupole coupling as compared to the 0^+ state, with χ_{bb} = 1.1(1) for 0+ and χ_{bb} = 1.4(1) for 0-. This difference in the quadrupole coupling may indicate a small change in the electric field gradient in the excited state and may provide useful information on changes in quadrupole coupling for the tunneling states.

b-dipole transitions

The b-dipole transitions were searched for, but not yet located. The problem is that the location of the b-dipole transitions will be very sensitive to possible tunneling, or internal motion present in the complex.

Quadupole coupling contant analysis

The alteration of nitrogen's electronic environment can be determined by comparing the experimental value of eQq_{aa} to nitrogen's experimental quadrupole tensor for ammonia. It is inferred that this alteration is due to the influence of the hydrogen bond. First, the angle between the c-axis of ammonia and the a-axis of the ammonia-formic acid complex was determined. Using this angle in the complex's a-b plane, ammonia's nitrogen quadrupole tensor was rotated from the ammonia principal axis system to the complex's principle axis system. This was accomplished with a matrix rotation program. The resulting calculated nitrogen quadrupole tensor using ammonia's value is -0.63 MHz. This is lower than the experimental eQq_{aa} values for the upper and lower states of the complex, which are -0.89 MHz and -0.96 MHz, respectively. This difference indicates that the electronic environment of ammonia's nitrogen is altered when in a dimeric interaction with formic acid. (KR)

5. Conclusions

The gas phase dimer composed of ammonia and formic acid has been investigated using microwave spectroscopy. The structure most consistent with the microwave measurements and fits to two different vibrational states, 0^+ and 0^-, is a double hydrogen-bonded dimer exhibiting internal motion. Our frequency range limited our ability to explore the coupling that may exist amongst other states. Future

experiments will probe the structure using isotopic substitution and more detailed searches for the transitions in the K_a=1 ladder of the 0^- state.

6. Acknowledgements

This material is based upon work supported by the National Science Foundation under Grant Nos. CHE-1057796 and CHE-1952289 at the University of Arizona. We thank Dr. Aaron Pejlovas for initial measurements on this complex.

Sb1---------

[1] P. R. Bunker and P. Jensen, "Molecular Symmetry and Spectroscopy", 2nd ed., NRC Research Press, Ottawa, (2006) ISBN: 0-7503-0941-5, doi:10.1063/1.2995676

[2] W.Li, L. Evangelisti, Q. Gou, W. Caminati, R. Meyer, 2019. Angew. Chem., Int. Ed. Engl., 58 (2019) 859-865. **https://doi.org/10.1002/anie.201812754**

[3] A.M. Daly, P.R. Bunker, S.G. Kukolich, J. Chem. Phys. 132 (2010) 201101/1–201101/3, https://doi.org/10.1063/1.3443508

[4] A.M. Daly, P.R. Bunker, S.G. Kukolich, J. Chem. Phys. 133 (2010) 079903/1, https://doi.org/10.1063/1.3472345

[5] A.M. Daly, K.O. Douglass, L.C. Sarkozy, J.L. Neill, M.T. Muckle, D.P. Zaleski, B.H. Pate, S.G. Kukolich, J. Chem. Phys. 135 (2011**)** 154304/1−154304/12, https://doi.org/10.1063/1.3643720

[6] Mackenzie, R.B., Dewberry, C.T. and Leopold, K.R., *J. Phys. Chem. A*, *118*(36), (2014) 7975-7985. https://doi.org/10.1021/jp507060w

[7] Evangelisti, L., Écija, P., Cocinero, E.J., Castaño, F., Lesarri, A., Caminati, W. and Meyer, R., 2012. *J. Phys. Chem. Lett.*, *3*(24) (2012) 3770-3775. https://doi.org/10.1063/1.1868552

[8] M.C.D. Tayler, B. Ouyang, B.J. Howard, J. Chem. Phys. 134 (2011) 054316/1–054316/9, https://doi.org/10.1063/1.3528688

[9] A.M. Daly, B.A. Sargus, S.G. Kukolich, J. Chem. Phys. 133 (2010) 174304/1–174304/6. https://doi.org/10.1063/1.3501356

[10] A.M Pejlovas, M. Barfield, S.G. Kukolich, Chem. Phys. Lett. 613 (2014) 86–89, https://doi.org/10.1016/j.cplett.2014.08.061

[11] A.M. Pejlovas, W. Lin, S.G. Kukolich, J. Chem. Phys. 143 (2015) 124311/1–124311/6, https://doi.org/10.1063/1.4931923

[12] A.M. Pejlovas, S.G. Kukolich, J. Mol. Spectrosc. 321 (2016) 1–4, https://doi.org/10.1016/j.jms.2016.01.011

[13] Ioannou, I.I. and Kuczkowski, R.L., 1994. *J. Phys. Chem*, *98*(9), (1994) 2231-2235. https://doi.org/10.1021/j100060a003

[14] Mackenzie, R.B., Dewberry, C.T. and Leopold, K.R., *J. Phys. Chem. A*, *120*(14), (2016) 2268-2273. https://doi.org/10.1021/acs.jpca.6b01500

[15] Nadykto, A.B. and Yu, F., *Chem. phys. lett.*, *435*(1-3) (2007) 14-18. https://doi.org/10.1016/j.cplett.2006.12.050

[16] Harold, S.E., Bready, C.J., Juechter, L.A., Kurfman, L.A., Vanovac, S., Fowler, V.R., Mazaleski, G.E., Odbadrakh, T.T. and Shields, G.C., 2022. *J. Phys. Chem. A*, *126*(10), (2022) 1718-1728. https://doi.org/10.1021/acs.jpca.1c10754

[17] Hellebust, S., O'Riordan, B. and Sodeau, J., 2007. J. Chem. Phys, *126*(8), (2007) 084702. https://doi.org/10.1063/1.2464082

[18] Löwdin, P.O., 1963. *Rev. Mod. Phys.*, *35*(3), (1963) 724. https://doi.org/10.1103/RevModPhys.35.724

[19] Lin, Y., Wang, H., Wu, Y., Gao, S. and Schaefer III, H.F. *Phys. Chem. Chem. Phys.*, *16*(14), (2014) 6717-6725. https://doi.org/10.1039/C3CP54904F

[20] Birer, Ö. and Havenith, M., 2009. *Ann. Rev. of Phys. Chem.*, *60*, (2009) 263-275. https://doi.org/10.1146/annurev.physchem.040808.090431

[21] Nelson Jr, D.D., Fraser, G.T. and Klemperer, W., 1985. J. Chem. Phys., *83*(12), (1985) 6201-6208. https://doi.org/10.1063/1.449566

[22] Nelson Jr, D.D., Klemperer, W., Fraser, G.T., Lovas, F.J. and Suenram, R.D., J. Chem. Phys. *87*(11), (1987) 6364-6372. https://doi.org/10.1063/1.453466

[23] Loeser, J.G., Schmuttenmaer, C.A., Cohen, R.C., Elrod, M.J., Steyert, D.W., Saykally, R.J., Bumgarner, R.E. and Blake, G.A., 1992. ., J. Chem. Phys. *97*(7), (1992) 4727-4749. https://doi.org/10.1063/1.463874

[24] Jing, A., Szalewicz, K. and van der Avoird, A., 2022. *Nature communications*, *13*(1), (2022) 1-8. https://doi.org/10.1038/s41467-022-28862-z

[25] Tackett, B.S., Karunatilaka, C., Daly, A.M. and Kukolich, S.G., *Organometallics*, *26*(8), (2007) 2070-2076.
https://doi.org/10.1021/om061027f

[26] Cox, A.P., Flynn, G.W. and Wilson Jr, E.B.J. Chem. Phys, *42*(9) (1965) 3094-3105.
https://doi.org/10.1063/1.1696386

[27] Gaussian 16, Revision C.01, Frisch, M. J.; Trucks, G. W.; Schlegel, H. B.; Scuseria, G. E.; Robb, M. A.; Cheeseman, J. R.; Scalmani, G.; Barone, V.; Petersson, G. A.; Nakatsuji, H.; Li, X.; Caricato, M.; Marenich, A. V.; Bloino, J.; Janesko, B. G.; Gomperts, R.; Mennucci, B.; Hratchian, H. P.; Ortiz, J. V.; Izmaylov, A. F.; Sonnenberg, J. L.; Williams-Young, D.; Ding, F.; Lipparini, F.; Egidi, F.; Goings, J.; Peng, B.; Petrone, A.; Henderson, T.; Ranasinghe, D.; Zakrzewski, V. G.; Gao, J.; Rega, N.; Zheng, G.; Liang, W.; Hada, M.; Ehara, M.; Toyota, K.; Fukuda, R.; Hasegawa, J.; Ishida, M.; Nakajima, T.; Honda, Y.; Kitao, O.; Nakai, H.; Vreven, T.; Throssell, K.; Montgomery, J. A., Jr.; Peralta, J. E.; Ogliaro, F.; Bearpark, M. J.; Heyd, J. J.; Brothers, E. N.; Kudin, K. N.; Staroverov, V. N.; Keith, T. A.; Kobayashi, R.; Normand, J.; Raghavachari, K.; Rendell, A. P.; Burant, J. C.; Iyengar, S. S.; Tomasi, J.; Cossi, M.; Millam, J. M.; Klene, M.; Adamo, C.; Cammi, R.; Ochterski, J. W.; Martin, R. L.; Morokuma, K.; Farkas, O.; Foresman, J. B.; Fox, D. J. Gaussian, Inc., Wallingford CT, 2016.

[28] A. D. Becke, *J. Chem. Phys.*, **98** (1993) 5648-52.
DOI: 10.1063/1.464913

[29] Grimme, S., *J. Comput.Chem.*, *27*(15), (2006) 1787-1799. https://doi.org/10.1002/jcc.20495

[30] R. Peverati and D. G. Truhlar *J. Phys. Chem. Lett.* **2** (2011) 2810-2817.
DOI: 10.1021/jz201170d

[31] J.-D. Chai and M. Head-Gordon, *Phys. Chem. Chem. Phys.*, **10** (2008) 6615-20.
DOI: 10.1039/B810189B

[32] Head-Gordon, M., Pople, J.A. and Frisch, M.J., *Chem. Phys. Lett.*, *153*(6), (1988) 503-506.
https://doi.org/10.1016/0009-2614(88)85250-3

[33] Y. Zhao and D. G. Truhlar, *Theor. Chem. Acc.*, **120** (2008) 215-41.
DOI: 10.1007/s00214-007-0310-x

[34] Hehre, W.J., Ditchfield, R. and Pople, J.A., *J. Chem. Phys*, *56*(5), (1972) 2257-2261.
https://doi.org/10.1063/1.1677527

[35] Hariharan, P.C. and Pople, J.A., *Theor. Chim. Acta*, *28*, (1973) 213-222.
https://doi.org/10.1007/BF00533485

[36] Krishnan, R.B.J.S., Binkley, J.S., Seeger, R. and Pople, J.A., *J. Chem. Phys*, *72*(1), (1980) 650-654.
https://doi.org/10.1063/1.438955

[37] Weigend, F., Furche, F. and Ahlrichs, R., *J. Chem. Phys*, *119*(24), (2003) 12753-12762.
https://doi.org/10.1063/1.1627293

[38] Kendall, R.A., Dunning Jr, T.H. and Harrison, R.J., *J. Chem. Phys*, *96*(9), (1992) 6796-6806.
https://doi.org/10.1063/1.462569

[39] Kendall, R.A., Dunning Jr, T.H. and Harrison, R.J., *J. Chem. Phys*, *96*(9), (1992) 6796-6806.
https://doi.org/10.1063/1.462569

[40] Kendall, R.A., Dunning Jr, T.H. and Harrison, R.J., *J. Chem. Phys*, *96*(9), (1992) 6796-6806. https://doi.org/10.1063/1.462569

[41] Dunning Jr, T.H., *J. Chem. Phys 90*(2), (1989) 1007-1023. https://doi.org/10.1063/1.456153

[42] Dunning Jr, T.H., *J. Chem. Phys 90*(2), (1989) 1007-1023. https://doi.org/10.1063/1.456153

[43] W.Li, L. Evangelisti, Q. Gou, W. Caminati, R. Meyer, 2019. Angew. Chem., Int. Ed. Engl., 58 (2019) 859-865. **https://doi.org/10.1002/anie.201812754**

[44] H.M. Pickett. J. Mol. Spectrosc. 148 (1991) 371–377, https://doi.org/10.1016/0022-2852(91)90393-0 <http://spec.jpl.nasa.gov/ftp/pub/calpgm/spinv.html>